ACS APPLIED MATERIALS & INTERFACES

Research Article

www.acsami.org

Effect of the Polymer Architecture on the Structural and Biophysical Properties of PEG–PLA Nanoparticles

Jean-Michel Rabanel,[†,‡] Jimmy Faivre,[‡] Soudeh F. Tehrani,[†] Augustine Lalloz,[†,‡] Patrice Hildgen,*[,†] and Xavier Banquy*[,‡]

[†]Laboratoire de Nanotechnologie Pharmaceutique, Faculté de Pharmacie, and [‡]Canada Research Chair on Bio-inspired Materials and Interfaces Faculté de Pharmacie, Université de Montréal, C.P. 6128, Succursale Centre-ville, Montréal, Québec H3C 3J7, Canada

Supporting Information

ABSTRACT: Polymers made of poly(ethylene glycol) chains grafted to poly(lactic acid) chains (PEG-*g*-PLA) were used to produce stealth drug nanocarriers. A library of comblike PEG-*g*-PLA polymers with different PEG grafting densities was prepared in order to obtain nanocarriers with dense PEG brushes at their surface, stability in suspension, and resistance to protein adsorption. The structural properties of nanoparticles (NPs) produced from these polymers by a surfactant-free method were assessed by dynamic light scattering, ζ potential, and transmission electron microscopy and found to be controlled by the amount of PEG present in the polymers. A critical transition from a solid NP structure to a soft particle with either a "micellelike" or a "polymer nanoaggregate" structure was observed when the PEG content was between 15 and 25% w/w. This structural transition was found to have a profound impact on the size of the NPs, their surface charge, their stability in suspension in the presence of salts, and the binding of proteins to the surface of the NPs. The arrangement of the PEG-*g*-PLA chains at the surface of the NPs was investigated by ^{1}H NMR and X-ray photoelectron spectroscopy (XPS). NMR results confirmed that the PEG chains were mostly segregated at the NP surface. Moreover, XPS and quantitative NMR allowed quantification of the PEG chain coverage density at the surface of the solid NPs. Concordance of the results between the two methods was found to be remarkable. Physical–chemical properties of the NPs such as resistance to aggregation in a saline environment as well as antifouling efficacy were related to the PEG surface density and ultimately to the polymer architecture. Resistance to protein adsorption was assessed by isothermal titration calorimetry using lysozyme. The results indicate a correlation between the PEG surface coverage and level of protein interactions. The results obtained lead us to propose such PEG-*g*-PLA polymers for nanomedicine development as an alternative to the predominant polyester–PEG diblock polymers.

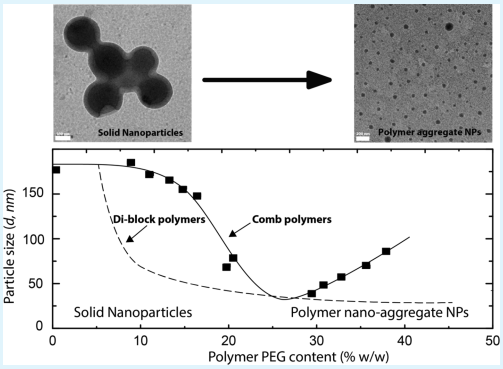

KEYWORDS: *poly(lactic acid), poly(ethylene glycol), nanoparticle, micellar particle, XPS, NMR, ITC*

INTRODUCTION

Polymeric nanoparticles (NPs) have been intensively investigated for their potential use as drug-delivery and targeting systems because of their stability in biological media, drug encapsulation and release capabilities, and compatibility with various routes of administration.[1−3] However, the high expectations generated by NP-based therapies (including liposomes, micelles, particles, etc.) are not currently matched by clinical successes. Only a handful of products have reached the market with, in several cases, limited improvement over preexisting formulations. These drug-delivery approaches are now seriously questioned, and many of their biological properties, such as organ clearance,[4] organ targeting and biodistribution,[5,6] ability to cross biological barriers,[7] ability to evade the complement system,[8] and ability to diffuse into tissue interstitium,[9] are under scrutiny. One of the most significant issues of NP-based systems is the limited accumulation of NPs at the pathological site, regardless of the nature of the NPs. It appears that only 5−10% of an intravenously injected dose of NPs does accumulate at the desired site, with 90−95% of the dose distributing nonspecifically to organs such as the liver and spleen.[10]

Many elements have been put forth to explain these disappointing results. One of them is the lack of systematic quantitative characterization of the properties of the particles used in drug delivery in spite of efforts put forward by many research teams.[11]

In order to fulfill their promise as drug-delivery systems, polymeric NPs should not only be composed of biocompatible, excretable, and/or degradable materials but also possess well-defined structures and adequate surface properties. Adequate surface properties can be conferred by a polymeric hydrophilic corona. In the case of polymeric NPs, such ahydrophilic corona can be formed during the NP fabrication process either by self-

Received: February 12, 2015
Accepted: April 24, 2015
Published: April 24, 2015

DOI: 10.1021/acsami.5b01423
ACS Appl. Mater. Interfaces 2015, 7, 10374−10385

Scheme 1. PEG-*g*-PLA Synthesis Scheme by Acyl Chloride Grafting

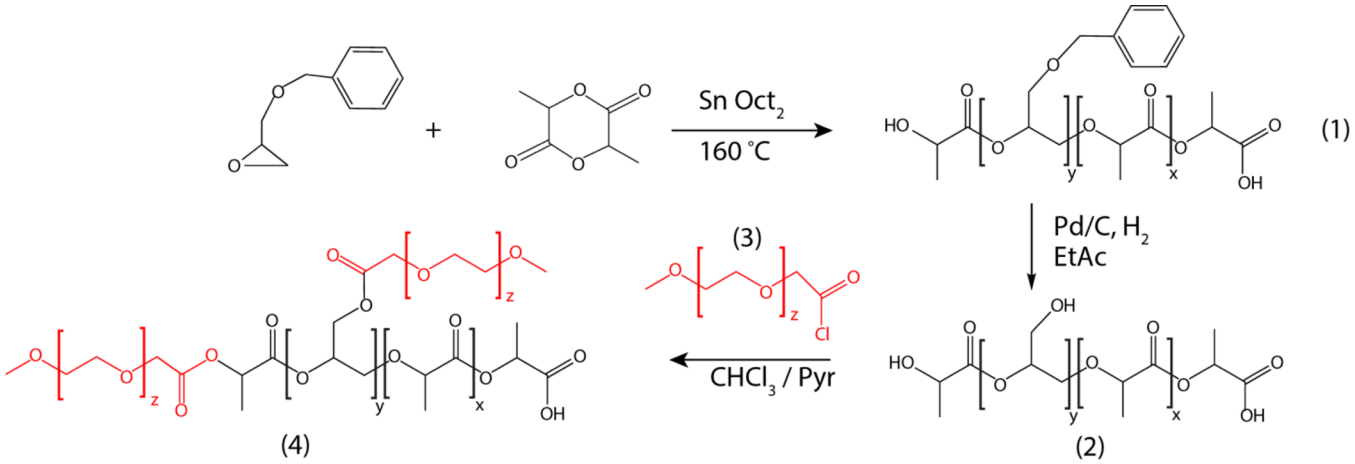

assembly of the polymer chains carrying hydrophilic moieties or by postgrafting of hydrophilic polymer chains at the surface of the NP. The self-assembly process, because of its simplicity, is by far the most commonly used method to produce NPs with a hydrophilic corona.

The use of poly(ethylene glycol) (PEG) as a corona-forming polymer is well established. The resistance of NPs to nonspecific absorption (opsonization) of plasmatic proteins is a key element in determining their fate in the human body. The antifouling properties of NPs control the half-life as well as other pharmacokinetic parameters of the NPs,[12] their targeting capabilities,[13,5] and their therapeutic action (pharmacodynamics). Denser PEG coatings have been shown to improve the diffusion of NPs in the extracellular matrix and across the mucosa barrier, which, in turn, should improve drug-delivery efficacy.[14,15] High resistance to protein adsorption as well as NP diffusion in complex media is obtained at high PEG surface densities, where the polymer chains are organized as brushes.[14,16] Resistance to protein adsorption has been extensively studied both at the fundamental level[17,18] and in the context of pharmaceutical sciences.[12]

While the effect of surface PEGylation on the biological outcome of nanobased drug-delivery systems has been extensively investigated in the literature, the correlations between the PEG copolymer architecture and its biological effects have yet to be explored. To date, the polymer architecture of choice is a linear diblock copolymer composed of a hydrophobic segment, usually a biodegradable polymer such as poly(lactic acid) (PLA) or poly(caprolactone) (PCL), and a hydrophilic segment, usually PEG.[19] The possible control of surface PEGylation and the particle structure by an alternative PEG copolymer architecture is an intriguing possibility that has received little attention.

Moreover, the PEG surface densities are often ill-characterized in the literature. This lack of characterization makes it difficult to compare the performance of different delivery systems and establish the optimal PEG surface density. In general, the PEG moieties are assumed to be completely segregated at the surface of the NPs based on indirect evidence such as an increase in the NP hydrodynamic diameter and a decrease of the ζ potential. Such an assumption leads to overestimation of the PEG density and incorrect appreciation of the PEG layer conformation. Direct quantification and assessment of the polymer conformation are not trivial, and the number of techniques suitable for polymeric NPs is indeed limited.[20] For example, ^{1}H NMR of NPs suspended in D_2O has been proposed for the first time by Hkrach et al. to qualitatively characterize PEG-*b*-PLA NPs.[21] Later, surface PEG quantification methods based on ^{1}H NMR have been proposed, relying on internal standards.[22,23] X-ray photoelectron spectroscopy (XPS), allowing analysis of NPs in the dried state, has also been proposed to semiquantify polymers attached at the surface of polystyrene NPs[24] and PLA NPs.[25−27]

We previously developed a family of comb-type copolymers having PEG chains branching along a linear polymeric backbone of PLA. This architecture had been proposed to increase the number of functionalities present on a single polymer chain and to help control the number and density of functionalities at the NP periphery. These polymers were used to produce stealth NPs in a one-step process that avoided the grafting of PEG chains after NP fabrication and facilitated purification. PEG segregation toward the surface was observed for these NPs.[27] However, assessment of the PEG density and optimization of the stealth behavior of the NPs are still lacking.

In this study, a library of branched/comb PEG-*g*-PLA with controlled PEG contents was synthesized in order to establish correlations between the polymer architecture and NP properties. A diblock PEG-*b*-PLA was also synthesized and used to compare the performance of the different polymers. The conformation of the PEG chains at the surface of the NPs was investigated by quantitative ^{1}H NMR and XPS. The performance of the PEGylated NPs was assessed by protein adsorption isotherms and colloidal stability assays. Correlations between the surface coverage afforded by PEG and the properties of the NPs allowed the establishment of criteria for the design and preparation of PEGylated polymeric NPs based on comb-shaped polymers.

EXPERIMENTAL METHODS

1. Materials. All chemicals were purchased from Sigma-Aldrich (Oakville, Ontario, Canada) unless otherwise stated in the text. Dilactide was recrystallized in toluene and dried overnight in a vacuum before use. Solvents were from Fisher Scientific (Whitby, Ontario, Canada) and were used as received.

2. Polymer Synthesis and Characterization. *a. Poly(ester-co-ether) Backbone Polymer Synthesis (Benzyl-g-PLA).* Polymer synthesis was carried out as previously described[28] with minor modifications. Briefly, random copolymerizations of D,L-dilactide and benzyl glycidyl ether (BGE) were obtained by ring-opening polymer-

DOI: 10.1021/acsami.5b01423
ACS Appl. Mater. Interfaces 2015, 7, 10374−10385

ization catalyzed by stannous 2-ethylhexanoate (molar ratio of 1:5000 relative to a lactic monomer) at 150 °C under an argon atmosphere and mechanical stirring for 6 h. At the end of the reaction, the crude polymer melt was dissolved in dichloromethane (DCM) and the polymer was precipitated in hexanes (HEX) twice to yield polymer **1** shown in Scheme 1 (total yield: 90−95%). The BGE/lactic acid ratio was varied from 0.5 to 3% to yield PLA backbone polymers with different benzyl side-chain densities.

*Example of Polymer **1**, Benzyl-g-PLA, at 1.1% Benzyl to Lactic Monomer Ratio.* FTIR (cm^{-1}): 3512.6, 2994.4, 2944.9, 2880.5, 1745.2, 1451.7, 1380.5, 1363.8, 1319.1, 1268, 1183.7, 1127.6, 1080.3, 1049, 956.1, 863.7, 746.9, 699.3. ^{1}H NMR (400 MHz, DMSO-d_6): δ 1.3−1.5 (m, 3H, CH_3), 4.48 (m 2H, CH_2), 3.58 (m, 2H), 4.2 (m, 2H), 5.2 (m, 1H, CH), 7.3 (m, 5H, benzylic). GPC: M_n 18500 g/mol; M_w 31700 g/mol.

b. Benzyl-g-PLA Debenzylation (HO-g-PLA). Alcohol pendant group was deprotected by catalytic hydrogenation in the presence of 5% palladium/carbon (1 g of carbon powder for each 1 mmol of benzyl group) in ethyl acetate under a constant hydrogen flow for 48 h. Palladium/carbon was removed on a filtration column (Celite Standard Super-Cel NF, Acros Organics, Thermo Fisher Scientific, USA). Polymer **2** was recovered after solvent evaporation, dissolution in DCM, precipitation in HEX, and drying under vacuum (Scheme 1). Complete removal of benzyl groups was confirmed by ^{1}H NMR (total yield: 95%).

*Example of Characterization of Polymer **2** after Debenzylation (HO-g-PLA, 1.1% Pendant OH).* FTIR (cm^{-1}): 2998.8, 2947.4, 1744.1, 1450.3, 1362, 1267.8, 1183.8, 1126.8, 1078.1, 954.7, 863.3, 745.2, 704.8. ^{1}H NMR (400 MHz, $CDCl_3$): δ 1.3−1.5 (m, 3H, CH_3), 3.58 (m, 2H), 4.19 (m, 2H), 5.2 (m, 1H, CH). GPC: M_n 16200 g/mol; M_w 28900 g/mol.

c. Methoxy-PEG Carboxyl (mPEG-COOH) Preparation. Methoxy-PEG-OH (mPEG-OH; 2 kDa) was oxidized by Jones reaction in acetone with 2.5 mol equiv of CrO_6 (equivalent to OH present), H_2SO_4, and H_2O for 4 h at room temperature under high-speed stirring. The reaction was stopped by the addition of 1 N HCl and isopropyl alcohol. Acetone was removed by evaporation. The polymer solution was then extracted and dialyzed to remove chromium. mPEG-COOH was recovered by freeze-drying as a white fluffy material. mPEG-COOH was kept in the presence of P_2O_5 under vacuum before use.

mPEG-COOH. FTIR (cm^{-1}): 3484.9, 2883.2, 2741.7, 1964.8, 1740.1, 1466.4, 1454.1, 1359.2, 1340.3, 1279.1, 1240.5, 1148, 1105.1, 1060.1, 946.4, 841.1, 667.5. ^{1}H NMR (400 MHz, $CDCl_3$): δ 3.38 (s, 3H, CH_3), 3.64 (m, 2H, CH_3), 4.16 (m, 2H, CH_2).

*d. Grafting of mPEG-COOH on Polymer **2** (PEG-Grafted PLA or PEG-g-PLA).* mPEG-COOH (2 kDa) was finally grafted onto PLA-OH polymers by acylation to yield PEG-*g*-PLA (polymer **3** in Scheme 1). Briefly, weighed PEG-COOH was incubated under stirring with an excess of thionyl chloride in $CHCl_3$ under an argon atmosphere for 2 h. After solvent removal and drying under vacuum, dry polymer **3** was added along with anhydrous pyridine in dry $CHCl_3$ stabilized by amylene and stirred for 24 h under an argon atmosphere. The PEG-*g*-PLA polymers were recovered after washing, precipitation, rotary evaporation of solvent, and drying. The PEG content in the polymers was controlled either by varying the BGE content in the polymer backbone, and thus available hydroxyl grafting sites, or by controlling the mPEG-COOH to OH-*g*-PLA ratio during the acylation reaction.

*Example of Characterization of PEGylated Polymer **4**, PEG-g-PLA.* FTIR (cm^{-1}): 2994.2, 2944.7, 2884.4, 2741.9, 2694.8, 1964.9, 1748.2, 1453.3, 1380.8, 1359.6, 1342.4, 1276, 1241.1, 1185.7, 1083.3, 1059.8, 962.4, 862.9, 841.9, 748.5, 698.8. ^{1}H NMR (400 MHz, $CDCl_3$): δ 1.3−1.5 (m, 3H, CH_3), 3.38 (s, 3H, CH_3), 3.65 (m, 2H CH_2), 4.18 (m, 1H), 4.35 (m, 2H), 5.2 (m, 1H, CH). GPC: M_n 16200 g/mol; M_w 28900 g/mol.

e. PEG Grafting by Dicyclohexylcarbodiimide (DCC) Coupling. Alternatively, the PEG chains were grafted by esterification with DCC as the coupling reagent and (dimethylamino)pyridine (DMAP) as the catalyst.[29] The number of available OH groups on OH-*g*-PLA (lateral and terminal) was estimated. A total of 1.1 equiv of mPEG-COOH was added and dissolved in DCM stabilized by amylene. DMAP and DCC (1 M in DCM) were added at a ratio of 1.2 mol equiv to the available OH groups. The reaction was kept under stirring for 48 h at room temperature.

PEGylated polymers were purified by filtration on a fritted glass (fine grade) funnel to remove *N*,*N*-dichlorourethane salt, followed by successive extractions with 0.5 M HCl (twice), saturated $NaHCO_3$, and finally Milli-Q water. The organic phase was dried with anhydrous sodium sulfate, and the polymers were precipitated in HEX. The polymers were dried under vacuum for 48 h before analysis.

The number of available OH groups on OH-*g*-PLA was calculated as follows: the number of lateral OH groups per chain was taken as the number of benzyl groups present before catalytic hydrogenation as determined by ^{1}H NMR. The number of terminal OH groups per gram of polymer was estimated based on M_n obtained by gel permeation chromatography (GPC). The PEG grafting calculations from NMR results are described in the Supporting Information (SI).

f. Diblock Synthesis (PEG-b-PLA). mPEG-OH (2 kDa) was used as a macroinitiator in the ring-opening polymerization of dilactide in the presence of $SnOct_2$, as previously described.[30]

FTIR (cm^{-1}): 2993, 2943.5, 2879.2, 1747.2, 1452, 1381, 1363.4, 1268.1, 1182.2, 1126.4, 1080, 1043.3, 956.4, 862.3, 752.1, 701.8. ^{1}H NMR (400 MHz, $CDCl_3$): δ 1.3−1.5 (m, 3H, CH_3), 3.38 (s, 3H CH_3), 3.65 (m, 2H), 5.2 (m, 1H, CH). GPC: M_n 20700 g/mol; M_w 29400 g/mol.

g. Polymer Characterization [NMR, GPC, and Fourier Transform Infrared (FTIR)]. The average molecular weights by weight (M_w) and by number (M_n) of the polymers were obtained by GPC in either tetrahydrofuran or $CHCl_3$. A Waters liquid chromatography system equipped with a refractive index detector, GPC columns (Styragel 5 μm, Phenomenex, USA), and *Breeze II* software (Waters Corp., Milford, MA) was used. The flow rate was set at 1 mL/min and the column temperature at 40 °C. Linear polystyrene standards (M_w 600−400000 g/mol) were used to construct the calibration curves.

IR spectra were recorded on a Nicolet iS10 FTIR (Thermo-Scientific, Canada) equipped with a SMART iTR attenuated total reflectance sampling accessory with a ZnSe plate. Data were acquired and analyzed using the OMNIC interface.

^{1}H and ^{13}C NMR and 2D ^{1}H/^{1}H (400 MHz) analyses were performed on a Bruker Advanced 300 or 400 MHz spectrometer (Bruker, Germany) and analyzed using *Mestrec* software. Samples were dissolved in either DMSO-d_6 or $CDCl_3$.

Differential scanning calorimetry (DSC) measurements were performed on a DSC Q2000 (TA Instruments, Waters LLC, USA) connected to a Q1000 RCS refrigerated cooling system (TA Instruments, Waters LLC, USA). Polymer and NP samples (approximately 5 mg) were placed in crimped aluminum pans. DSC analysis was carried out under a nitrogen flow by heating the samples from −40 to +80 °C at 10 °C/min, holding for 1 min, cooling to −40 °C at 20 °C/min, and reheating to 80 °C at 10 °C/min. T_g (glass transition temperature) and the PEG fusion peak were determined from the second heating run in the case of the polymers and from the first heating run in the case of the NP samples. Analysis was done using the TA Instruments *Universal Analysis 2000*, version 4.5A (TA Instruments, Waters LLC, USA) software.

The polymer density was determined using a helium Ultrapycnometer 1000 (Quantachrome Instrument, Boynton Beach, FL). A total of 10 measurements were averaged.

3. NP Preparation and Characterization. *a. Nanoprecipitation.* NPs were prepared by a nanoprecipitation method without the addition of surfactants. Polymers were dissolved in acetone at concentrations ranging from 5 to 20 mg/mL [0.5−2% (w/v)] and injected at a constant flow of 30 mL/h in an aqueous phase (organic to aqueous phase ratio of 1:5) under stirring. After solvent evaporation and dialysis (SpectraPor membranes, 6−8 kDa, Spectra Laboratories, USA) against a 100-fold volume of Milli-Q water (Millipore Canada Ltd., Etobicoke, Ontario, Canada) for 12 h, twice; the suspension was kept at 4 °C until use.

b. Concentration of NP Preparation. NP preparations were concentrated for NMR and microcalorimetry experiments using either

DOI: 10.1021/acsami.5b01423
ACS Appl. Mater. Interfaces 2015, 7, 10374−10385

tangential flow filtration or reverse osmosis. Tangential flow filtration was used for NPs having an average diameter of 70−150 nm. It was carried out using a polysulfone filtration column (pore 0.05 μm, Spectra Laboratories, USA) at a flow rate of 3 mL/min for 2 h. This approach typically yielded a 5−7-fold concentration increase. As described elsewhere,[31] particle batches of NPs with sizes below 70 nm were concentrated by reverse osmosis against a 500 kDa dextran solution (10 g/100 mL in Milli-Q water), with dialysis membranes of 6−8 kDa (SpectraPor, Spectra Laboratories). Typically, concentration increases of 10−20-fold were obtained over a 72−96 h period. The concentrates were examined for aggregation and size change by dynamic light scattering (DLS).

c. Size Measurements. The NP size was determined by photon correlation spectroscopy on a Malvern Zetasizer (Malvern, Worcester, U.K.) at a diffraction angle of 173° in triplicate in either Milli-Q water or 10 mM phosphate-buffered saline (PBS; pH 7.4).

d. ζ-Potential Measurements. NPs (0.3 mg) were suspended in 1 mL of 5 mM NaCl and placed in a disposable folded capillary cell to measure the ζ potential on a Malvern Zetasizer (Malvern, Worcester, U.K.). Measurements were done in triplicate.

e. Determination of the NP Concentration. A fixed volume of a vortexed NP suspension (500 μL) was placed in a tared Eppendorf tube and freeze-dried. The tube was weighed again after complete drying of the material to obtain the weight of the NPs.

4. XPS Surface Analysis. The NPs were freeze-dried without any cryoprotectant to obtain a fine fluffy powder. The powder was pressed on double-sided tape and mounted onto a sample rod. XPS survey analysis was performed on a Excalab MK II (VG Scientific, Thermo Scientific) with a Mg Kα X-ray source (1253.6 eV) powered at 200 W, an electron takeoff angle of 0°, and steps of 1.0 eV for an energy pass of 1000 eV. High-resolution spectra were acquired on a Kratos Axis Ultra (Kratos Analytical, Manchester, U.K.) with a Mg Kα X-ray source used at 120 W (12 kV and 10 mA), with steps of 0.05 eV for an energy pass of 20 eV. A flood gun was used to offset the surface charges.

The relative atomic percentage was calculated using the *Advanced* software (VG Scientific, ThermoFisher) from the low-resolution spectra. The high-resolution spectra were analyzed by curve deconvolution of the C 1s and O 1s signals on *Advanced* software (VG Scientific, ThermoFisher). The background was subtracted by the Shirley method using the Wagner sensitivity factor table. All spectra were calibrated on the C−C aliphatic carbon binding energy peak set at 285.0 eV to compensate for surface charging effects. Peak fitting was performed as previously described[25] and based on data obtained for pure PLA and PEG.[32] The conversion of relative atomic percentages to mass percentages and to PEG surface densities is described in detail in the SI (section S5).

5. Determination of the PEG Surface Density by NMR Analysis. *a. Determination of the PEG Proton Relaxation Time.* The relaxation time of the PEG signal in D_2O was first assessed. D_1 was then set at 5 s during the quantitative experiments, as previously reported for PEG-DSPE.[33]

b. Total and Surface PEG Quantification. The PEG content at the surface of the NPs was determined by two methods. The first method consisted of producing the NPs directly in deuterated solvents. Briefly, 20 mg of polymer was dissolved in 1 mL of acetone-*d* and injected into 5 mL of deuterium oxide [with 0.75% 3-(trimethylsilyl)propionic-*2,2,3,3-d*$_4$ sodium salt as the internal standard] under stirring. After acetone evaporation on a rotary evaporator, 1 mL of the nanosuspension was transferred to an NMR tube and analyzed by ^{1}H NMR (AV400 Advanced, Bruker, Germany). Another 1 mL of the nanosuspension was freeze-dried in a tared Eppendorf tube in order to determine the mass concentration of the NPs for PEG surface density calculations. The same sample was dissolved in $CDCl_3$ and analyzed by ^{1}H NMR (AV400 Advanced, Bruker, Germany) in reference to the internal standard tetramethylsilane and a PEG calibration curve in $CDCl_3$ to determine the total PEG content of the sample. The second method relied on the dilution of a concentrated NP suspension in D_2O. The methods to concentrate the NP suspensions and determine the NP concentration were described earlier. Amounts of 200 and 500 μL of concentrated NP suspension were added respectively to 800 and 500 μL of deuterium oxide (with an internal standard) and analyzed. NP suspensions in D_2O and H_2O/D_2O were analyzed by ^{1}H NMR (AV400 Advanced, Bruker, Germany). Quantifications were conducted in reference to an mPEG-OH 2 kDa calibration curve and an internal standard peak intensity.

c. PEG Surface Density Evaluation by NMR Calculation. See the SI for more details on PEG chain surface density calculations.

6. Transmission Electron Microscopy (TEM). *a. Sample Preparation for TEM.* NP suspensions in Milli-Q water (1−2 mg/mL) were deposited on carbon films on 400 mesh copper grids (Electron Microscopy Sciences, Hatfield, PA) as droplets of about 2−4 μL. The droplets were allowed to sit for 5 min before excess liquid was removed with a filter paper. Grids were allowed to air-dry for 1−2 h before image acquisition. No staining procedure was used.

b. TEM Image Acquisition. TEM image acquisition was done in bright-field mode in a JEM-2100F field-emission electron microscope (Jeol Ltd., Tokyo, Japan) equipped with a sample holder cooled by liquid nitrogen (Gatan Inc., Warrendale, PA). The grids were maintained at −170 °C throughout the acquisition with a temperature controller (Smart Set model 900 cold stage controller; Gatan Inc., Warrendale, PA). In brief, the grids were introduced into the microscope column under vacuum. Liquid nitrogen was added to the sample holder and the temperature recorded. The sample was exposed to the electron beam only after the temperature had reached −170 °C. The acceleration voltage was set at 200 kV. Images were recorded with a digital camera at low electron dose to prevent damage to the heat-sensitive particles (current densities between 5 and 15 pA/cm^2). Images were acquired at a 0° angle. In a few cases, images were also acquired at either 15 or 30° angles. Images were transferred, adjusted, and analyzed using the *ImageJ* software.[21]

7. Colloidal Stability in Saline. The colloidal stability was evaluated by measuring the critical coagulation concentration (CCC) by DLS. Different NaCl solutions with concentrations from 10 mM to 2 M were tested. A known volume of NPs, V, was added to 1 mL of a saline solution and rapidly stirred. The final NP concentration was 1 mg of NP/mL. The particle size was immediately measured for 15 min at 2 min intervals (three measurements of four runs at 25 °C). The volume of each NP formulation to add to the saline solution was estimated using eq 1.

$$V = \frac{4\pi r^3 d N_{\text{part}}}{3C} \quad (1)$$

where V is the volume of the formulation pipetted to adjust the particle number in the sample, r is the mean NP radius as measured in Milli-Q water by DLS, d is the density of the NPs (g/cm^3), N_{part} is the targeted number of NPs in the solution (namely, 4.7×10^{14} NPs/mL), and C is the NP concentration in the stock suspension (g/mL).

8. Protein Binding Assays. *a. Protein Binding Isotherms.* Protein binding isotherms were measured by incubating a fixed amount of NPs with increasing concentrations of either fluorescent bovine serum albumin (BSA) or fluorescent lysozyme (LYZ). BSA coupled with fluorescein isothiocyanate (BSA-FITC) was from Sigma-Aldrich. LYZ coupled with rhodamine isothiocyanate (RITC) was prepared as follows. A total of 1 g of egg white LYZ was dissolved in 160 mL of borate buffer (pH 8.3). RITC (100 mg) was dissolved in 40 mL of the same buffer. The two solutions were mixed at a LYZ/RITC molar ratio of 2.8 and stirred for 24 h at 10 °C. The protein was purified by repeated dialysis (SpectraPor RC membrane, 6−8 kDa cutoff, Spectrum Laboratories) against Milli-Q water to remove unreacted RITC and freeze-dried. NP batches were prepared in PBS (15 mM, pH 7.4) as described above and dialyzed against PBS before use. The NP concentration was determined by freeze-drying 1 mL of NP suspension, and the NP diameter was measured by DLS to calculate the total surface area (nm^2/mg of NP). Stock solutions of BSA-FITC and LYZ-RITC were prepared in PBS at 1 mg/mL and serially diluted. Aliquots (200 μL) of either 2 mg/mL NP suspensions or PBS (as control) were placed in vials with 40 μL of fluorescent

DOI: 10.1021/acsami.5b01423
ACS Appl. Mater. Interfaces 2015, 7, 10374−10385

Table 1. Polymer Characteristics Depending on Their Architecture and Grafting Method

polymer architecture	grafting method	M_n[a] of OH-g-PLA (g/mol)	M_w[a] of OH-g-PLA (g/mol)	PDI	grafting ratio of PEG chain/LA (% 100)[b]	PEG chain/PLA chain	M_w[c] of polymer (g/mol)	% w/w PEG
comb	DCC	18500	28300	1.53	0.31	0.8	29890	**7.9**
comb	DCC	24300	40300	1.66	0.473	1.6	43520	**11.6**
comb	DCC	18500	28300	1.53	0.63	1.62	31540	**14.9**
comb	DCC	24330	33890	1.39	0.63	2.13	38150	**14.9**
comb	DCC	13400	19820	1.48	0.89	1.66	23100	**19.8**
comb	DCC	18500	28300	1.53	0.93	2.39	33080	**20.5**
comb	DCC	14180	23990	1.69	1.26	2.48	28950	**25.9**
comb	DCC	22200	30700	1.38	1.5	4.63	39950	**29.4**
comb	EDC	15700	22700	1.45	1.6	3.49	29680	**30.8**
comb	DCC	17000	25300	1.49	1.76	4.16	33600	**32.8**
comb	DCC	15700	22700	1.45	2	4.36	31420	**35.7**
comb	acyl chloride	23600	34400	1.46	0.33	1.08	36560	**8.0**
comb	acyl chloride	23600	34400	1.46	0.56	1.84	38070	**11.1**
comb	acyl chloride	22500	29800	1.32	0.75	2.34	34490	**13.3**
comb	acyl chloride	22 500	29800	1.32	0.96	3	35800	**16.5**
diblock	ROP[d]	NA	NA		0.4	1	23800	***5.1***

[a]Determined by GPC. [b]Determined by ^{1}H NMR. [c]Calculated based on the GPC results. [d]Ring-opening polymerization.

protein solution. The final protein concentrations ranged between 0 and 160 μg/mL (0−2400 nM) for BSA and 0 and 130 μg/mL (0−8840 nM) for LYZ. The solutions were incubated in an orbital shaker at 37 °C for 24 h under constant stirring at 50 rpm and then centrifuged at 20000*g* for 20 min. The pellets were washed and dissolved in 1.3 mL of dimethylformamide. Fluorescence was measured at λ_{ex} = 490 nm and λ_{em} = 530 nm for BSA-FITC and λ_{ex} = 550 nm and λ_{em} = 570 nm for LYZ-RITC. The measurements were recorded with a F2710 fluorescence spectrophotometer (Hitachi, Tokyo, Japan). The amount of proteins adsorbed to the NPs was calculated using a calibration curve and expressed as the number of proteins adsorbed per nm^2 of NP (protein/nm^2), as a function of the free-protein concentration in solution (nM), the difference between the initial protein concentration and the concentration removed from the solution by protein binding on the NP surface. Every test was performed in triplicate, and the results are reported as mean value ± standard error.

b. Isothermal Titration Calorimetry (ITC). The heat of adsorption (Q) of LYZ on the surface of the NPs was measured by microcalorimetry. The experiments were carried out on a Microcal VP-ITC instrument (GE Healthcare Life Sciences, Pittsburgh, PA). The volume of the sample cell was 1.4 mL. NP suspensions [5−10 g/L (0.1−10 nM) in 15 mM PBS (pH 7.4)] were placed in the sample cell under constant stirring (350 rpm). A LYZ solution (Sigma-Aldrich, St. Louis, MO) at 1 g/L in 15 mM PBS (pH 7.4) was filtered, degassed, and placed in an injection syringe. Titrations were performed by adding 1 × 2 and 12 × 20 μL of a LYZ solution (total volume of 242 μL). The equilibration time between injections was set to 1200 s, and the temperature was kept constant at 25 °C. The reference cell was filled with 15 mM PBS (pH 7.4). The heat of dilution of LYZ was determined by titrating LYZ over 15 mM PBS (pH 7.4). The heat of dilution of LYZ was used as the reference and subtracted from all of the binding isotherms. In a control experiment, a LYZ solution [1 g/L in 15 mM PBS (pH 7.4)] was titrated over a solution of mPEG-OH (2 kDa) in 15 mM PBS (pH 7.4).

RESULTS AND DISCUSSION

1. Polymer Synthesis and Characterization. Copolymer synthesis was carried out according to a modified procedure based on the copolymerization of dilactide with BGE (Scheme 1). Compared to the original approach developed in our laboratory,[28] the present procedure avoided the oxidation steps necessary to insert carboxyl moieties on the pendant groups. These oxidation steps were found to significantly affect the PLA backbone integrity with a substantial decrease in M_w. In the present approach, catalytic hydrogenation of the benzyl pendant groups under mild conditions was able to recover the hydroxyl groups (see section S1 in the SI). No decrease in M_w was seen by GPC (see Table S1 in the SI for information on the PLA backbone synthesis), suggesting that this approach maintains the integrity of the polymer backbones and allows better control over the molecular mass of the copolymer chain. Different PEGylated polymer batches were synthesized with varying PEG contents (polymer structure in Scheme 1) and characterized, as shown in Table 1. Grafting of PEG was performed by either an acyl chloride reaction (Scheme 1)[28] or DCC/DMAP coupling (Scheme S1 in the SI).[29] The PLA backbone chain length was chosen to be long enough to achieve NP structural integrity yet short enough to ensure adequate speed of hydration, erosion, and release of active ingredients from the polymeric matrix. This aspect is further developed in an upcoming paper dealing with hydrophobic drug encapsulation.

With the DCC coupling method, the grafting ratios obtained are in accordance with esterification of the secondary terminal OH PLA group as well as the primary pendant alcohol groups (see Table S1 in the SI for the calculated number of available OH in each polymer batch). However, with the acyl chloride method, the grafting ratios were consistent with a grafting occurring predominately on the pendant alcohol groups only.

2. Preparation and Characterization of NPs. *a. Particle Size.* Figure 1A shows the evolution of the NP diameter with the PEG content in the polymer (for the same PEG chain length of 2 kDa). Our results show that, from 5 to 15% w/w PEG, large solid particles are formed with sizes that tend to decrease as the PEG content increases (Figure 1A). Above 15% w/w, significantly smaller particles are formed, as observed by both DLS (Figure 1A) and TEM imaging (Figure 2). Starting from 25% w/w PEG, the trend is reversed and the size of the particles increases linearly with the PEG content. This increase in size could result from a stretching of the PEG chains due to a higher surface PEG chain density[34] or to an increase in the aggregation number of the particles.

The transition from large NPs to smaller particles was found to occur in a narrow range of the PEG content situated between 15 and 20% w/w. Such a sharp transition contrasts

DOI: 10.1021/acsami.5b01423
ACS Appl. Mater. Interfaces 2015, 7, 10374−10385

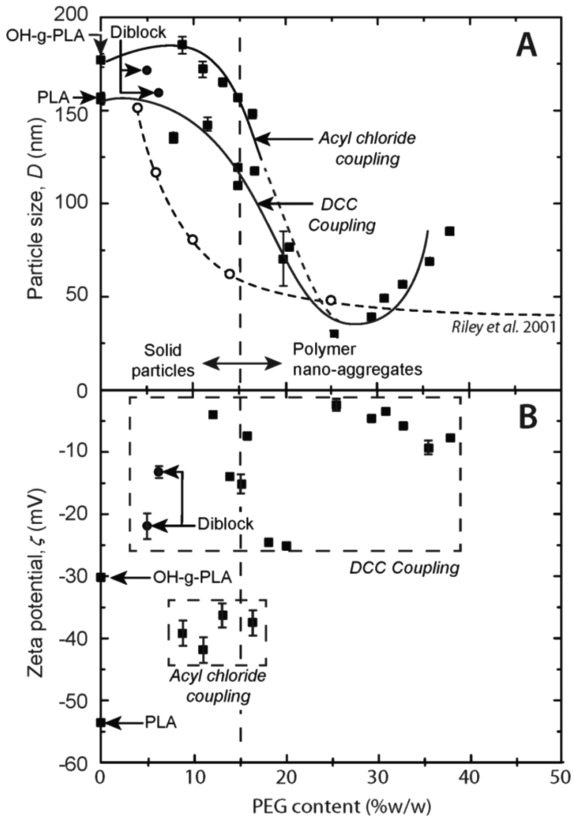

Figure 1. (A) Particle size dependence over the total PEG content. Solid squares represent particle batches produced for this study, while empty circles reproduce data from Riley et al.[35] obtained with a diblock PEG-*b*-PLA polymer with a PEG segment of 5000 g/mol. (B) ζ-potential dependence over the total PEG. The NP ζ potential measured in 5 mM NaCl increases sharply with the PEG content in the particle regime and stays constant in the micellar regime. Lines represent the fourth-order polynomial fit (R^2 = 0.91).

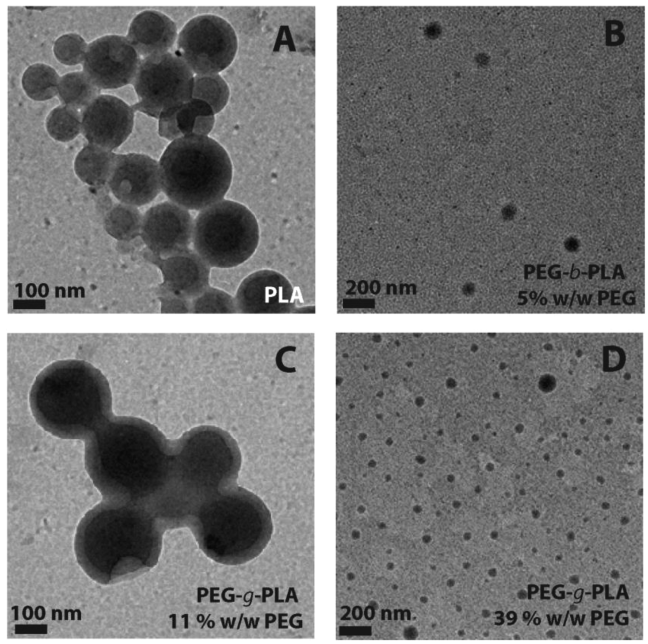

Figure 2. Representative cryo-TEM images of NPs fabricated from PLA, PEG-*b*-PLA diblock copolymer, and PEG grafted copolymers: (A) PLA NPs; (B) diblock PEG-*b*-PLA NPs; (C) solid PEG-*g*-PLA NPs with a PEG content of 11% w/w; (D) PEG-*g*-PLA polymer nanoaggregate with a PEG content of 38% w/w.

with the smooth/continuous transition reported for diblock polymers (see Figure 1A).[35] Such differences in behavior demonstrate the importance of the polymer architecture on NP structuration. The linear increase in size in the higher PEG content regime (i.e., >20% w/w PEG content) was also reported by Logie et al., who studied the effect of the PEG content of comb-shaped polymers (from 0.6 to 6 PEG chains per polymer) on the micelle stability and size by DLS and TEM.[36]

b. ζ Potential. The ζ potential of the NPs produced using PEGylated polymers prepared via the acyl chloride grafting method was found to be largely negative and inferior to −30 mV (Figure 1B). On the other hand, ζ of the NPs produced with PEGylated polymers synthesized via the DCC coupling method was found to be significantly higher, ranging from −20 to 0 mV. Polymers exhibiting PEG chains at the end of the PLA backbone (diblocks or polymer synthesized by the DCC method) present values of ζ much closer to neutrality compared to polymers exhibiting PEG chains well distributed on the PLA backbone (polymer synthesized by the acyl chloride method). These findings suggest that the position of the PEG chain in the PLA backbone plays a crucial role in the composition of the NP−medium interface. Independent of the synthetic method used, it appears that ζ tends to increase from −40 mV to almost 0 mV with the PEG content, which confirms the screening of the surface charges on the NP surface by PEG chains.

c. Structure and Morphology of Particles. Effect of the PEG Content and Polymer Architecture. The relationship between the NP formation process and the NP internal structure is still poorly understood. With the goal of improving our knowledge of such a relationship, we performed cryo-TEM imaging of the NPs. Cryo-TEM images confirmed the existence of two particle structures, i.e., solid core particles at PEG contents below 15% w/w (Figure 2A,C) and "polymer nanoaggregates" or soft particles at PEG contents above 15% w/w (Figure 2D). Soft particles were also obtained for the diblock polymers (Figure 2B). The particle sizes measured by cryo-TEM were in agreement with DLS analysis (using a size distribution by number). The PLA and PEG-*g*-PLA solid particles displayed an apparent core−shell structure (Figure 2A,C). Pustulka et al. reported a similar core−shell structure for NPs made of diblock PEG-*b*-PLGA prepared by flash nanoprecipitation and encapsulating hydrophobic derivatives of paclitaxel.[37] The authors suggested that the observed structure was the result of a drug-rich core surrounded by a PLGA shell and a PEG corona. In our case, however, the structures were observed regardless of the presence of hydrophilic polymer blocks or encapsulated hydrophobic compounds. We found that the shape of the core−shell interface and its position could be changed by simply tilting the substrate during imaging. Such changes in the shape and position were found to be consistent with a solid NP in flat contact with the substrate (see Figure S11 in the SI). Polymer nanoaggregate particles did not exhibit any core−shell-like features on cryo-TEM images (Figure 2B,D), which is an indication of significant deformation of the NPs on the substrate upon deposition on the carbon grids. Such significant deformation is favored by the lower glass transition temperature (T_g) of the most PEGylated polymers compared to PLA (see the calorimetric data in Table S4 in the

DOI: 10.1021/acsami.5b01423
ACS Appl. Mater. Interfaces 2015, 7, 10374−10385

SI). The PEG corona itself is neither dense enough nor thick enough to be seen by TEM, and other analytical methods should be used for its characterization.

Nature of the Particles. NPs produced from comb-shaped polymers with low PEG content (<15% w/w) were observed as solid particles, while NPs produced from polymers with higher PEG content (>15%) were observed as soft "micellelike" or "polymer nanoaggregate" particles (Figure 2). From TEM imaging, it appears that the latter particles are soft (at room temperature) and that they flatten upon dehydration during sample preparation and under vacuum. The structural organization of the polymeric chains forming the particles containing over 15% w/w PEG is not clearly defined yet. By analogy with other block copolymer NPs, the term "micellelike" could be used to describe them.[38,39] However, such a term may not be appropriate because it defines a thermodynamically stable structure, which is certainly not the case of the present NPs, which appear as kinetically frozen, as already mentioned previously.[19,40] A micellar phase is characterized by the independence of the micelle size over the polymer concentration as well as a narrow micelle size distribution. Both properties were not observed with the polymers under study because we found large polydispersity (PDI) for the polymer nanoaggregate (PDI $\geq$ 0.25), as shown in Table S6 in the SI. Particle preparations using different polymer concentrations in the organic stock solution showed significant variations of the NP size indicative of a NP formation mechanism more related to precipitation/aggregation than micellization (data not shown). The PEG polymer content could also affect the polymer solution viscosity in the organic solvent, which is a determinant of the particle size produced by nanoprecipitation (Figure S6 in the SI).

Effect of the PEG Grafting Method. We found differences in the NP properties whether PEGylation was achieved by DCC or acyl chloride coupling reactions, even at similar PEG contents. NPs prepared from polymers obtained by DCC coupling appeared to be similar to NPs prepared from the diblock polymer in terms of the ζ potential and TEM morphology. NPs prepared from acyl chloride polymers seemed similar to plain PLA and OH-*g*-PLA NPs. The differences are mostly due to the difference in the polymer architecture obtained by the two coupling methods. Acyl chloride coupled polymers have well-distributed PEG branches characteristic of the comblike architecture. On the other hand, DCC polymers, even if they have PEG lateral grafted chains, have properties more related to diblock polymers because of the PEG segment is present at the PLA chain end. These structural differences might explain why NPs prepared with DCC polymers have sizes and ζ more closely related to those obtained with the diblock polymers compared to the acyl chloride polymers.

3. Calorimetric Properties of PEGylated Polymers and NPs. As already reported by Sant et al.,[37,41] T_g of PEG-*g*-PLA polymers depends strongly on the PEG content in the polymer (Table S4 in the SI). The first and second runs of DSC scans of representative polymers are shown in Figures S9 and S10 in the SI. The main difference between the first and second runs was the disappearance of the polymer chain relaxation endotherm.[37,41] T_g of the polymers was determined as the midpoint of the extrapolated tangent of the baseline and was located between −5 and +30 °C (Table S4 in the SI).

DSC scans of freeze-dried NPs presented striking differences compared to those of the bulk polymers. The presence of PEG dispersed in PLA was evidenced by a reduction of T_g in PEG-*g*-PLA NPs compared to PLA NPs and by the absence of a PEG fusion endotherm (data not shown). T_g shifts have also been observed in drug-loaded NPs as a result of polymer−drug interactions.[42] The presence of PEG chains in the particle core was also supported by the NMR quantification data, as will be detailed below (Figure 3). T_g recorded for all NPs appeared

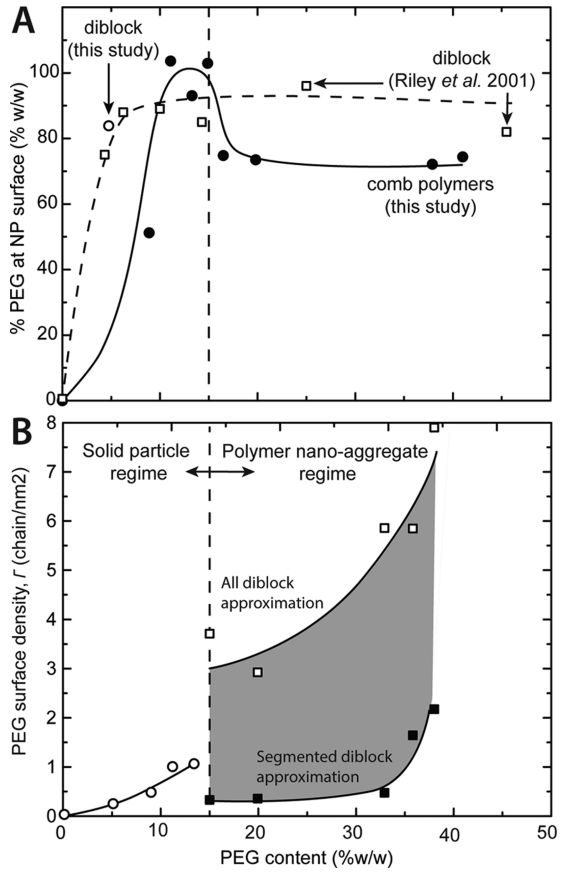

Figure 3. (A) Evolution of the percentage of PEG at the surface of the NPs and (B) PEG surface densities determined by quantitative NMR as a function of the PEG content in the polymer for solid *and* polymer nanoaggregate particles. In part B, open squares represent the calculated PEG surface density base on the "all diblock" approximation; closed squares represent the calculated PEG surface density base on the "segmented diblock" approximation. Error bars are smaller than the symbols used.

independent of the PEG content (Table S4 in the SI). This could result from a near-constant amount of PEG, acting as a plasticizer, in the NP core.

4. Quantification of the PEG Distribution at the NP Surface and in Its Core. *a. NMR Studies.* The presence of PEG at the NP surface was confirmed by ^{1}H NMR analysis in D_2O. In D_2O, the PEG signals are sharp and well-defined, indicating that the PEG chains are at the surface of the NPs and highly hydrated, while the PLA signals cannot be resolved (an example NMR spectrum is shown in Figure S8 in the SI).[21,37] The absence of PLA signals supports a strongly dehydrated PLA core characteristic of solid NPs. No PLA signal was seen for the polymer nanoaggregates also, suggesting a kinetically frozen core with no exchange of unimers with the surrounding media. For instance, NPs made with PEG-*b*-PLA diblocks have been shown to display a solid core when the molar mass of the

DOI: 10.1021/acsami.5b01423
ACS Appl. Mater. Interfaces 2015, 7, 10374−10385

Table 2. NMR and XPS Quantification of the PEG Surface Density of Solid Particles

		^{1}H NMR[a]					
		NPs prepared in D_2O		NPs concentrated and suspended in D_2O		XPS[a]	
polymer architecture	PEG content (% w/w)	diameter[b] (nm)	surface density (PEG/nm^2)	diameter[b] (nm)	surface density (PEG/nm^2)	diameter[b] (nm)	surface density (PEG/nm^2)
comb	8.9	87.6	0.5	157.1	0.45	128.3	0.47
		95	0.55			149.1	0.43
						101.1	0.42
						100.9	0.39
comb	11.1			134.8	0.97	87.5	0.57
						99.53	0.91
comb	13.3	116.8	1.2	132.8	1.04	135.4	1.03
		99.5	1.07			101.1	1.02
comb	16.5			113.8	0.88	97.6	1.02
diblock	5	83.9	0.22			74.4	0.30
		64.3	0.22			67.7	0.32

[a]Density calculations are detailed in the SI, sections S5 and S6. [b]Average size based on a distribution by number.

PLA hydrophobic segment was above 6000 g/mol, while a liquid core was found for hydrophobic blocks below 4000 g/mol.[22] For the NPs obtained at a PEG content >15% w/w having a kinetically frozen core, the use of "polymer nanoaggregates" is justified to designate them.[40]

The exact PEG percentage at the surface and PEG surface density was quantified by NMR. Two sample preparation methods were tested, namely, nanoprecipitation of the dissolved polymer in deuterated acetone into deuterium oxide and preparation of NPs in pure H_2O followed by their dilution in D_2O. The first method has the advantage of producing ready-to-analyze particles and of generating NMR spectra exempt of a broad H_2O peak that could interfere with integration of the PEG peak (Figure S8 in the SI). However, this method produced NPs with smaller diameters compared to nanoprecipitation in H_2O (Table 2) and NP preparation with residual organic solvent. D_2O and H_2O differ in surface tension, viscosity, and density, parameters that affect the nanoprecipitation process. The second method used closely reproduces the normal preparation procedure of the NPs. However, it requires concentration of the NP suspension after nanoprecipitation, which can generate a potential problem in the control of the NP size and which complicates quantitative analysis by NMR due to the presence of H_2O in the suspension medium. To minimize this last issue, the suspensions were concentrates so as to minimize residual H_2O in the sample. The stability of the nanosuspensions after particle concentration by either tangential filtration or reverse osmosis was assessed by DLS (see Table S6 in the SI for the sizes of the NPs measured before and after concentration).

The percentage of PEG found at the surface of the NPs was calculated as the ratio of the mass of PEG detected by NMR over the total PEG content present in the sample (see Figure 3A). The percentage of PEG found at the surface increased with the PEG content in the solid particle regime (i.e., between 9 and 20% w/w of PEG) and reached a maximum at around 90%. In the polymer nanoaggregate regime (i.e., when the PEG content was increased above 20% w/w), the PEG percentage found at the surface of the NPs decrease to about 75% and remained constant thereafter, revealing that a significant portion of the PEG chains were located inside the particle core (Figure 3A). In contrast, Riley et al. found a higher percentage (80−100%) of total PEG at the surface of the NPs prepared with diblock polymers of different PLA block sizes (Figure 3A).[43] Small-angle neutron scattering studies also confirmed the presence of PEG in the particle core for polyester−PEG diblock polymer NPs.[44] In light of these differences, it appears that the comblike architecture is imposing constraints on the migration of PEG chains toward the surface during NP formation.

The PEG surface density, Γ, was calculated using eq 2

$$\Gamma = \frac{R^3}{R_c^{\,2}} \times \%\ \mathrm{PEG(surface)} \times \%\ \mathrm{PEG(polymer)} \times \rho_p \frac{N_A}{M_w} \quad (2)$$

where R is the hydrodynamic radius of the NP, R_c is the radius of the core of the NP, ρ_p refers to the polymer density, M_w is its molecular weight, and N_A is Avogadro's number. % PEG(surface) refers to the fraction of polymer at the surface of the NP, while % PEG(polymer) refers to the PEG content in the polymer.

^{1}H NMR analysis of NPs suspended in D_2O allowed determination of the surface density of PEG, Γ (Table 2 and Figure 3B). For solid particles, we used the approximation $R \simeq R_c$ and found that Γ increased with the PEG content almost linearly to reach a value of $\Gamma \simeq 1$ chain/nm^2 at 15% w/w PEG content, which is well above the theoretical brush regimen threshold of 0.01−0.005 chain/nm^2. Other calculation methods were tested, leading to similar results (see section S6 in the SI in ref 20). Of note, the PEG surface density was found to be insensitive to PEG contents between 9 and 15% w/w.

In the micellar/polymer aggregate regime (i.e., at PEG contents >15−20% w/w), accurate density values could not be obtained given that the core radius, R_c, was not experimentally available in this regime. R_c was estimated using the star polymer approximation for polymeric micelles.[45] We used two possible effective architectures to calculate the number of hydrophilic and hydrophobic segments. In the first approximation, we considered all of the ethylene oxide monomers per chain to form a single hydrophilic block. We called this first approximation the "all-diblock" approximation. In the second approximation, each PEG segment was considered as an individual chain associated with a fraction of the PLA chain. We called this second approximation the "segmented diblock" approximation. Both approximations allowed upper and lower

DOI: 10.1021/acsami.5b01423
ACS Appl. Mater. Interfaces 2015, 7, 10374−10385

bound values for Γ to be obtained as shown in Figure 3B (respectively represented by open and closed squares).

Despite the large differences between the upper and lower boundaries defined by these two approximations, they both predict an eventual increase of Γ with the PEG content. Our approach does not allow identification of any dramatic change in the PEG surface density at the transition from solid particles to polymer nanoaggregates, as was observed for the percentage of PEG at the surface of the NPs and for the NP diameter.

b. XPS Studies. Qualitatively, high-resolution XPS spectra of NPs showed an enrichment of PEG at the surface compared to the PEG-*g*-PLA polymer bulk, as calculated in weight percent based on chemical bond quantification (see Figure S7 and Table S3 in the SI). These data support the orientation of the PEG moieties toward the surface of the NPs and are in accordance with the NMR results.[27]

Calculations based on the C 1s high-resolution spectra give a semiquantitative result that can be translated into the PEG surface density because the particle volume analyzed is a two-component substrate (PLA and PEG). Details of the calculation method can be found in the SI (section S5). Two main assumptions were used in the calculation: (1) the polymer volumes analyzed by XPS were homogeneous and (2) all of the PEG chains detected and quantified were localized at the surface of the NPs.

The PEG surface density results obtained by XPS are presented in Table 2. The results are found to be in close agreement with the NMR results, in spite of the difference in state of the NPs (dry vs wet state) and the different assumptions made in the calculation methods. The PEG detected by XPS belongs to a layer of about 10 nm in depth at the surface of the NPs. As mentioned above, we assumed for the sake of calculation that the PEG chains detected were all at the surface of the NPs. However, it cannot be excluded that some of this PEG is buried just underneath the surface. This is why discrepancies can be expected between the XPS and NMR results.

Of note, XPS analysis was not performed on polymer nanoaggregate particles because the radii of the particles decrease rapidly. Assuming that the layer accessible to XPS analysis is 10 nm in depth, the volume examined by XPS is about 35% of the total volume of a particle of 150 nm diameter. For particles of about 50 nm diameter, this volume percentage increases to about 80%. In the latter case, XPS analysis becomes less pertinent to giving insight about the surface properties of the NPs.

5. Colloidal Stability Studies. The colloidal stability of NP suspensions was assessed by monitoring their aggregation kinetics in a salt solution (Figure 4 and inset). The CCC at which rapid aggregation of the particles occurred was used as stability criteria. CCC was determined when rapid aggregation occurred, i.e., when the rate of aggregation was found to be positive.

In the solid particle regime, the CCC increased slightly with the PEG content of the polymer. Above a PEG content of 20% w/w, the CCC increased dramatically, indicating that the polymer nanoaggregates are extremely stable. In that regime, the colloidal stability was maintained even at very high salt concentrations (>2 M NaCl). The extreme stability of the particles can be explained by the presence of strong repulsive steric forces originating from the presence of a dense layer of PEG chains in the brush conformation, as suggested by our findings. Also, it is worth noting that at such high salt

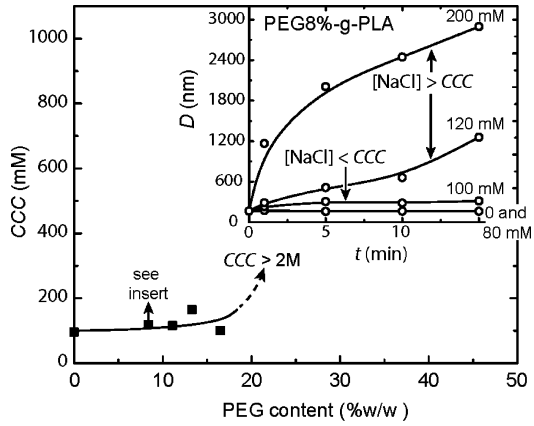

Figure 4. CCC of NP suspensions of PEG-*g*-PLA polymers. Inset: Aggregation kinetics of NPs composed of PEG8%-*g*-PLA in the presence of different NaCl concentrations as measured by DLS. Error bars are smaller than the symbols used.

concentrations other repulsive forces due to ion correlations may be expected to play a role as well.

6. Protein Binding Studies. *a. Protein Absorption Isotherms.* Human serum albumin (HSA) is the most abundant protein in serum (35 g/L). In vivo it plays a role in creating a protein corona at the surface of the particles, promoting their recognition by macrophage cells and their elimination. BSA is a protein similar to HSA. BSA has a molecular weight of 66.5 kDa, a diameter of about 3.8 nm, and an isoelectric point of 4.7−5.1, making it a negatively charged protein at physiological pH. LYZ has a molecular weight of 14703 g/mol and an isoelectric point of 11, making it a positively charged protein at physiological pH.

As a reference, the theoretical monolayer protein values were calculated using surface values of 45 and 12.6 nm^2 for BSA and LYZ, respectively (see Table S5 in the SI). A BSA monolayer thus corresponds to a surface density of 0.022 BSA/nm^2, while the value is 0.08 LYZ/nm^2 for a LYZ monolayer. Experimentally, the binding of LYZ yielded a nonsaturated isotherm of absorption (Figure 5). The LYZ surface densities obtained were below the monolayer surface density. In contrast, BSA binding saturated rapidly. Again, the values obtained were

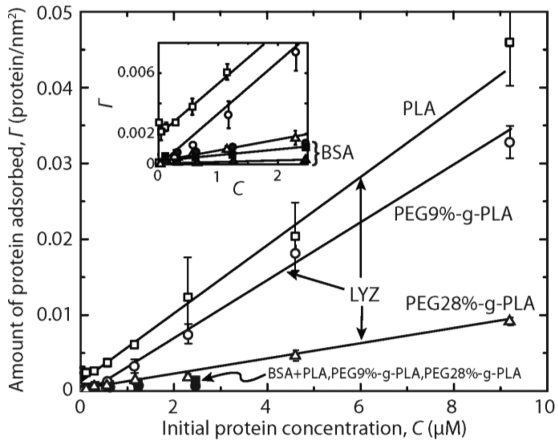

Figure 5. Adsorption isotherms of BSA and LYZ at the surface of the NPs. For all NPs tested, BSA adsorbed at the surface of the NPs to a lesser extent than LYZ. Inset: Enlarged portion of the adsorption isotherms. Lines represent linear fits (R^2 = 0.93).

DOI: 10.1021/acsami.5b01423
ACS Appl. Mater. Interfaces 2015, 7, 10374−10385

far below the protein monolayer surface density. At any given protein concentration, LYZ adsorbed to the NPs 10−15 times more than BSA did. This difference could be attributed to electrostatic interactions favoring binding of LYZ to the negatively charged NP surface (Figure 2b). Polymer nanoaggregates appeared more efficient at preventing BSA and LYZ binding than solid NPs. The protein binding values decreased with an increase in the PEG content of the polymers composing the NPs (Figure 5).

b. ITC. BSA Binding Studies. The binding of proteins at the surface of the NPs was also studied by ITC. This technique is well suited to evaluate particle stealthness, as previously proposed.[46,47] However, initial adsorption studies with BSA failed to produce a significant thermal signal (data not shown). The surface hydrophilicity, particle concentration (1−50 mg/mL), temperature (15−25 °C), and protein concentration (0.5−2 mg/mL) were varied but still did not yield a significant signal. At the pH of the experiments and in the absence of divalent cations in the PBS buffer used, BSA was negatively charged and had limited attraction to the negatively charged surface of the NPs. Lindman et al. studied the binding of a range of proteins (including human albumin) on hydrophilic acrylamide-based NPs by ITC. Contrary to our findings, the authors did record exothermic signals generated by the adsorption of proteins at the surface of the NPs.[46]

Knowing that protein binding did occur (as evidenced by the adsorption isotherms shown in Figure 5 and by the change in the ζ potential of the NPs measured after ITC experiments; see Table S7 in the SI), the absence of a calorimetric signal indicates that the protein adsorption energy and binding constants are very weak. Lindman et al. hypothesized that protein adsorption occurs without enthalpy change; i.e., the adsorption is strictly entropy-driven because of the release of H_2O from the NP and protein surfaces.[46]

LYZ Binding Studies. When LYZ was used as a model protein, an exothermic signal could be recorded by ITC, confirming the existence of stronger interactions between the NPs and positively charged protein. This observation is in agreement with the adsorption isotherms presented in Figure 5. The complex shapes of the thermograms shown in Figure 6 indicate that a more complex mechanism of interaction than simple electrostatic interactions between the NPs and proteins is at play. For the PEGylated NPs, the maximum exothermic values reached in the binding isotherm decreased with increasing PEG content in the NP. This indicates that the strength of the interactions between the surface of the NPs and LYZ decreased as the PEG surface density increased. Moreover, the saturation concentration, defined as the inflection point of the binding isotherm, increased with the PEG content until the signal reached the baseline (Figure 6). Interestingly, NPs with PEG contents higher than 15% w/w did not present any detectable calorimetric interactions. This is in agreement with the adsorption isotherms. Of note, visual examination of the samples after completion of the ITC experiments revealed flocculation of the NPs containing less than 15% w/w PEG. Such bridging of the NPs in the presence of LYZ was not observed in the case of polymer nanoaggregate particles.

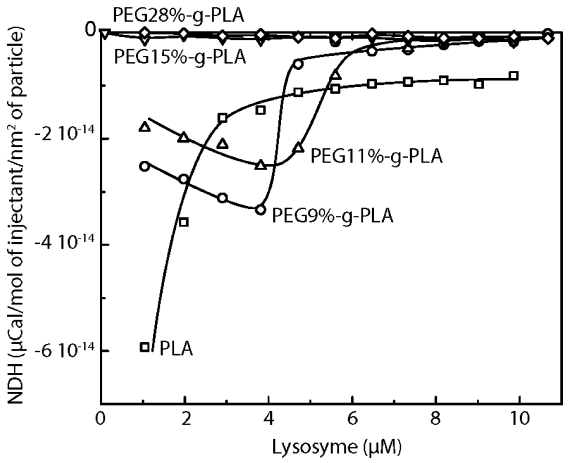

Figure 6. ITC assays performed by the addition of a 1 mg/mL LYZ solution to NPs with different PEG contents. The integrated calorimetric signal was normalized to the NP surface.

The contribution of the interaction between LYZ and PEG to the observed results was investigated. The ITC experiment trying to evidence interactions between free PEG chains in solution and LYZ in similar concentration conditions did not show any significant signal (data not shown). This result demonstrates the absence of direct interactions between LYZ and the PEG chains of the NP corona. This result actually argues in favor of penetration of the protein through the PEG brush and direct interaction between LYZ and the PLA core of the NP. This "primary adsorption" is favored by the small size of the protein (Table S4 in the SI). Secondary (inside the brush) and tertiary (on the top of the brush) adsorptions are less likely to occur because of the lack of an interaction signal between PEG and LYZ.[48]

As shown herein, comb polymers could be advantageous alternatives to other polymer architectures to confer high protein resistance to NPs. This is supported by another study showing that a PLL-*g*-PEG polymer with a 20-kDa PLL backbone and 3.5 2-kDa PEG pendant chains is conferring higher protein resistance to cationic metallic surfaces than similar polymers with other architectures.[49] In another recent study, increased stability in a biological medium was also shown for micelles made from comb-shaped polymers with increasing PEG grafting densities.[36]

CONCLUSION

The organization of the polymer chains of NPs prepared by nanoprecipitation seems to differ whether the polymers are comb-shaped or diblock. The characterization carried out in this study shows a discontinuity in the size and ζ-potential dependence when a critical PEG content is reached. The PEG content (% w/w) determines two apparent regimes: a solid particle regime and a polymer nanoaggregate regime. Interestingly, we found that only about 75% of the total PEG content was present at the surface of the NPs for both solid particles and polymer nanoaggregates. The implications of having PEG chains present inside the particle core remain to be investigated, but it may be that the PEG chains would play a role in drug encapsulation and release. Finally, protein adsorption and calorimetric studies indicate that the comb architecture could be advantageous over other polymer architectures to confer high protein resistance to NPs.

This paper represents a starting point toward the development of a nanocarrier platform for drug delivery. We are currently formulating these polymers for the delivery of active compounds to the central nervous system. All of the NP properties reported in the present paper are very relevant to evaluating the potential use of the NPs as drug carriers. We

DOI: 10.1021/acsami.5b01423
ACS Appl. Mater. Interfaces 2015, 7, 10374−10385

believe that the NP morphology, colloidal stability, and protein adsorption are key design parameters that have to be evaluated before encapsulating any active compounds in the formulation. This paper reveals that these key properties are intrinsically linked to the polymer architecture and composition.

■ ASSOCIATED CONTENT

Supporting Information

^{1}H NMR, GPC, and FTIR characterizations of representative polymers, methods of calculations of surface densities from quantitative ^{1}H NMR and XPS, supplementary TEM images, and information on NP batch characterization before and after concentration. The Supporting Information is available free of charge on the ACS Publications website at DOI: 10.1021/acsami.5b01423.

■ AUTHOR INFORMATION

Corresponding Authors

*E-mail: patrice.hildgen@umontreal.ca. Tel.: +1 (514) 343-6448.

*E-mail: xavier.banquy@umontreal.ca. Tel.: +1 (514) 343-2470.

Author Contributions

The manuscript was written through contributions of all authors. All authors have given approval to the final version of the manuscript.

Notes

The authors declare no competing financial interest.

■ ACKNOWLEDGMENTS

J.-M.R. thanks the "Fonds de Recherche du Québec, Nature et Technologie" (FRQ-NT, Government of Québec, Canada) and the Faculty of Pharmacy of the Université de Montréal for doctoral fellowships. X.B. acknowledges support by the Canada Research chair program of the government of Canada. P.H. acknowledges support by FRQ-NT (Québec, Canada). The authors thank Suzie Poulin and Josianne Lefebvre (Laboratoire d'analyse de surface, École Polytechnique, Montréal, Québec, Canada) for their help with XPS analysis. TEM imaging was performed at the "Centre de Caractérisation Microscopique des Matériaux" of the École Polytechnique (Montréal, Québec, Canada) with the help of Jean-Philippe Massé. Dr. Mohammad Taghi Savoji, Prof. Julian Zhu, Sylvain Essiembre, and Pierre Ménard-Tremblay are acknowledged for their help in GPC and DSC analysis. Johanne Habr's technical assistance in NP batch preparations is also acknowledged. Help with the optimization of NP preparation and concentration procedures by Prof. V. Gaêlle Roullin is greatly appreciated. Editing of this article by Dr. M. H. Dufresne is greatly acknowledged.

■ REFERENCES

(1) Brigger, I.; Dubernet, C.; Couvreur, P. Nanoparticles in Cancer Therapy and Diagnosis. *Adv. Drug Delivery Rev.* **2012**, *64* (Supplement), 24−36.

(2) Danhier, F.; Ansorena, E.; Silva, J. M.; Coco, R.; Le Breton, A.; Préat, V. PLGA-Based Nanoparticles: An Overview of Biomedical Applications. *J. Controlled Release* **2012**, *161*, 505−522.

(3) Hrkach, J.; Von Hoff, D.; Ali, M. M.; Andrianova, E.; Auer, J.; Campbell, T.; De Witt, D.; Figa, M.; Figueiredo, M.; Horhota, A.; Low, S.; McDonnell, K.; Peeke, E.; Retnarajan, B.; Sabnis, A.; Schnipper, E.; Song, J. J.; Song, Y. H.; Summa, J.; Tompsett, D.; Troiano, G.; Van Geen Hoven, T.; Wright, J.; LoRusso, P.; Kantoff, P. W.; Bander, N. H.; Sweeney, C.; Farokhzad, O. C.; Langer, R.; Zale, S. Preclinical Development and Clinical Translation of a PSMA-Targeted Docetaxel Nanoparticle with a Differentiated Pharmacological Profile. *Sci. Transl. Med.* **2012**, *4*, 128ra39.

(4) Bertrand, N.; Leroux, J.-C. The Journey of a Drug-Carrier in the Body: An Anatomo-Physiological Perspective. *J. Controlled Release* **2012**, *161*, 152−163.

(5) Ruenraroengsak, P.; Cook, J. M.; Florence, A. T. Nanosystem Drug Targeting: Facing up to Complex Realities. *J. Controlled Release* **2010**, *141*, 265−276.

(6) Kwon, I. K.; Lee, S. C.; Han, B.; Park, K. Analysis on the Current Status of Targeted Drug Delivery to Tumors. *J. Controlled Release* **2012**, *164*, 108−114.

(7) Rabanel, J. M.; Aoun, V.; Elkin, I.; Mokhtar, M.; Hildgen, P. Drug-Loaded Nanocarriers: Passive Targeting and Crossing of Biological Barriers. *Curr. Med. Chem.* **2012**, *19*, 3070−3102.

(8) Moghimi, S. M.; Andersen, A. J.; Hashemi, S. H.; Lettiero, B.; Ahmadvand, D.; Hunter, A. C.; Andresen, T. L.; Hamad, I.; Szebeni, J. Complement Activation Cascade Triggered by PEG-PL Engineered Nanomedicines and Carbon Nanotubes: The Challenges Ahead. *J. Controlled Release* **2010**, *146*, 175−181.

(9) Jain, R. K.; Stylianopoulos, T. Delivering Nanomedicine to Solid Tumors. *Nat. Rev. Clin. Oncol.* **2010**, *7*, 653−664.

(10) Bae, Y. H.; Park, K. Targeted Drug Delivery to Tumors: Myths, Reality and Possibility. *J. Controlled Release* **2011**, *153*, 198−205.

(11) Crist, R. M.; Grossman, J. H.; Patri, A. K.; Stern, S. T.; Dobrovolskaia, M. A.; Adiseshaiah, P. P.; Clogston, J. D.; McNeil, S. E. Common Pitfalls in Nanotechnology: Lessons Learned from NCI's Nanotechnology Characterization Laboratory. *Integr. Biol.* **2013**, *5*, 66−73.

(12) Vonarbourg, A.; Passirani, C.; Saulnier, P.; Benoit, J. P. Parameters Influencing the Stealthiness of Colloidal Drug Delivery Systems. *Biomaterials* **2006**, *27*, 4356−4373.

(13) Salvati, A.; Pitek, A. S.; Monopoli, M. P.; Prapainop, K.; Bombelli, F. B.; Hristov, D. R.; Kelly, P. M.; Aberg, C.; Mahon, E.; Dawson, K. A. Transferrin-Functionalized Nanoparticles Lose Their Targeting Capabilities When a Biomolecule Corona Adsorbs on the Surface. *Nat. Nano* **2013**, *8*, 137−143.

(14) Nance, E. A.; Woodworth, G. F.; Sailor, K. A.; Shih, T.-Y.; Xu, Q.; Swaminathan, G.; Xiang, D.; Eberhart, C.; Hanes, J. A Dense Poly(Ethylene Glycol) Coating Improves Penetration of Large Polymeric Nanoparticles within Brain Tissue. *Sci. Transl. Med.* **2012**, *4*, 149ra119.

(15) Ensign, L. M.; Schneider, C.; Suk, J. S.; Cone, R.; Hanes, J. Mucus Penetrating Nanoparticles: Biophysical Tool and Method of Drug and Gene Delivery. *Adv. Mater.* **2012**, *24*, 3887−3894.

(16) Gref, R.; Luck, M.; Quellec, P.; Marchand, M.; Dellacherie, E.; Harnisch, S.; Blunk, T.; Muller, R. H. 'Stealth' Corona−Core Nanoparticles Surface Modified by Polyethylene Glycol (PEG): Influences of the Corona (PEG Chain Length and Surface Density) and of the Core Composition on Phagocytic Uptake and Plasma Protein Adsorption. *Colloids Surf., B* **2000**, *18*, 301−313.

(17) Degennes, P. G. Conformation of Polymers Attached to an Interface. *Macromolecules* **1980**, *13*, 1069−1075.

(18) Jeon, S. I.; Lee, J. H.; Andrade, J. D.; Degennes, P. G. Protein Surface Interactions in the Presence of Polyethylene Oxide. 1. Simplified Theory. *J. Colloid Interface Sci.* **1991**, *142*, 149−158.

(19) Letchford, K.; Burt, H. A Review of the Formation and Classification of Amphiphilic Block Copolymer Nanoparticulate Structures: Micelles, Nanospheres, Nanocapsules and Polymersomes. *Eur. J. Pharm. Biopharm.* **2007**, *65*, 259−269.

(20) Rabanel, J.-M.; Hildgen, P.; Banquy, X. Assessment of Peg on Polymeric Particles Surface, a Key Step in Drug Carrier Translation. *J. Controlled Release* **2014**, *185*, 71−87.

(21) Hrkach, J. S.; Peracchia, M. T.; Bomb, A.; Lotan, N.; Langer, R. Nanotechnology for Biomaterials Engineering: Structural Characterization of Amphiphilic Polymeric Nanoparticles by ^{1}H NMR Spectroscopy. *Biomaterials* **1997**, *18*, 27−30.

(22) Heald, C. R.; Stolnik, S.; Kujawinski, K. S.; De Matteis, C.; Garnett, M. C.; Illum, L.; Davis, S. S.; Purkiss, S. C.; Barlow, R. J.;

DOI: 10.1021/acsami.5b01423
ACS Appl. Mater. Interfaces 2015, 7, 10374−10385

Gellert, P. R. Poly(Lactic Acid)−Poly(Ethylene Oxide) (PLA−PEG) Nanoparticles: NMR Studies of the Central Solidlike PLA Core and the Liquid PEG Corona. *Langmuir* **2002**, *18*, 3669−3675.
(23) Garcia-Fuentes, M.; Torres, D.; Martín-Pastor, M.; Alonso, M. J. Application of NMR Spectroscopy to the Characterization of PEG-Stabilized Lipid Nanoparticles. *Langmuir* **2004**, *20*, 8839−8845.
(24) Brindley, A.; Davis, S. S.; Davies, M. C.; Watts, J. F. Polystyrene Colloids with Surface-Grafted Polyethylene Oxide as Model Systems for Site-Specific Drug Delivery: I. Preparation and Surface Chemical Characterization Using SIMS and XPS. *J. Colloid Interface Sci.* **1995**, *171*, 150−161.
(25) Shakesheff, K. M.; Evora, C.; Soriano, I.; Langer, R. The Adsorption of Poly(Vinyl Alcohol) to Biodegradable Microparticles Studied by X-Ray Photoelectron Spectroscopy (XPS). *J. Colloid Interface Sci.* **1997**, *185*, 538−547.
(26) Lacasse, F. X.; Hildgen, P.; McMullen, J. N. Surface and Morphology of Spray-Dried PEGylated PLA Microspheres. *Int. J. Pharm.* **1998**, *174*, 101−109.
(27) Sant, S.; Poulin, S.; Hildgen, P. Effect of Polymer Architecture on Surface Properties, Plasma Protein Adsorption, and Cellular Interactions of PEGylated Nanoparticles. *J. Biomed. Mater. Res., Part A* **2008**, *87A*, 885−895.
(28) Nadeau, V.; Leclair, G.; Sant, S.; Rabanel, J. M.; Quesnel, R.; Hildgen, P. Synthesis of New Versatile Functionalized Polyesters for Biomedical Applications. *Polymer* **2005**, *46*, 11263−11272.
(29) Neises, B.; Steglich, W. Simple Method for the Esterification of Carboxylic Acids. *Angew. Chem., Int. Ed. Engl.* **1978**, *17*, 522−524.
(30) Quesnel, R.; Hildgen, P. Synthesis of PLA-*b*-PEG Multiblock Copolymers for Stealth Drug Carrier Preparation. *Molecules* **2005**, *10*, 98−104.
(31) Vauthier, C.; Cabane, B.; Labarre, D. How to Concentrate Nanoparticles and Avoid Aggregation? *Eur. J. Pharm. Biopharm.* **2008**.
(32) Beamson, G.; Briggs, D. *High Resolution XPS of Organic Polymers the Scienta Esca300 Database*; John Wiley & Sons Ltd.: West Sussex, England, 1992.
(33) Vernooij, E. A. A. M.; Gentry, C. A.; Herron, J. N.; Crommelin, D. J. A.; Kettenes-van den Bosch, J. J. ^{1}H NMR Quantification of Poly(Ethylene Glycol)−Phosphatidylethanolamine in Phospholipid Mixtures. *Pharm. Res.* **1999**, *16*, 1658−1661.
(34) de Gennes, P. G. Polymers at an Interface; a Simplified View. *Adv. Colloid Interface Sci.* **1987**, *27*, 189−209.
(35) Riley, T.; Stolnik, S.; Heald, C. R.; Xiong, C. D.; Garnett, M. C.; Illum, L.; Davis, S. S.; Purkiss, S. C.; Barlow, R. J.; Gellert, P. R. Physicochemical Evaluation of Nanoparticles Assembled from Poly(Lactic Acid)−Poly(Ethylene Glycol) (PLA−PEG) Block Copolymers as Drug Delivery Vehicles. *Langmuir* **2001**, *17*, 3168−3174.
(36) Logie, J.; Owen, S. C.; McLaughlin, C. K.; Shoichet, M. S. PEG-Graft Density Controls Polymeric Nanoparticle Micelle Stability. *Chem. Mater.* **2014**, *26*, 2847−2855.
(37) Pustulka, K. M.; Wohl, A. R.; Lee, H. S.; Michel, A. R.; Han, J.; Hoye, T. R.; McCormick, A. V.; Panyam, J.; Macosko, C. W. Flash Nanoprecipitation: Particle Structure and Stability. *Mol. Pharm.* **2013**, *10*, 4367−4377.
(38) Riley, T.; Govender, T.; Stolnik, S.; Xiong, C. D.; Garnett, M. C.; Illum, L.; Davis, S. S. Colloidal Stability and Drug Incorporation Aspects of Micellar-Like PLA−PEG Nanoparticles. *Colloids Surf., B* **1999**, *16*, 147−159.
(39) Zhang, L.; Eisenberg, A. Multiple Morphologies and Characteristics of "Crew-Cut" Micelle-Like Aggregates of Polystyrene-*b*-Poly(Acrylic Acid) Diblock Copolymers in Aqueous Solutions. *J. Am. Chem. Soc.* **1996**, *118*, 3168−3181.
(40) Johnson, B. K.; Prud'homme, R. K. Mechanism for Rapid Self-Assembly of Block Copolymer Nanoparticles. *Phys. Rev. Lett.* **2003**, *91*, 118302.
(41) Sant, S.; Thommes, M.; Hildgen, P. Microporous Structure and Drug Release Kinetics of Polymeric Nanoparticles. *Langmuir* **2008**, *24*, 280−287.
(42) Essa, S.; Rabanel, J. M.; Hildgen, P. Effect of Aqueous Solubility of Grafted Moiety on the Physicochemical Properties of Poly(D,L-Lactide) (PLA) Based Nanoparticles. *Int. J. Pharm.* **2010**, *388*, 263−273.
(43) Riley, T.; Heald, C. R.; Stolnik, S.; Garnett, M. C.; Illum, L.; Davis, S. S.; King, S. M.; Heenan, R. K.; Purkiss, S. C.; Barlow, R. J.; Gellert, P. R.; Washington, C. Core−Shell Structure of PLA−PEG Nanoparticles Used for Drug Delivery. *Langmuir* **2003**, *19*, 8428−8435.
(44) Yang, B.; Lowe, J. P.; Schweins, R.; Edler, K. J. Small Angle Neutron Scattering Studies on the Internal Structure of Poly(Lactide-*co*-Glycolide)-*block*-Poly(Ethylene Glycol) Nanoparticles as Drug Delivery Vehicles. *Biomacromolecules* **2014**.
(45) Halperin, A. Polymeric Micelles: A Star Model. *Macromolecules* **1987**, *20*, 2943−2946.
(46) Lindman, S.; Lynch, I.; Thulin, E.; Nilsson, H.; Dawson, K. A.; Linse, S. Systematic Investigation of the Thermodynamics of HSA Adsorption to *N*-Iso-Propylacrylamide/*N*-*tert*-Butylacrylamide Copolymer Nanoparticles. Effects of Particle Size and Hydrophobicity. *Nano Lett.* **2007**, *7*, 914−920.
(47) Cedervall, T.; Lynch, I.; Lindman, S.; Berggard, T.; Thulin, E.; Nilsson, H.; Dawson, K. A.; Linse, S. Understanding the Nanoparticle−Protein Corona Using Methods to Quantify Exchange Rates and Affinities of Proteins for Nanoparticles. *Proc. Natl. Acad. Sci. U. S. A.* **2007**, *104*, 2050−2055.
(48) Halperin, A. Polymer Brushes That Resist Adsorption of Model Proteins: Design Parameters. *Langmuir* **1999**, *15*, 2525−2533.
(49) Kenausis, G. L.; Vörös, J.; Elbert, D. L.; Huang, N.; Hofer, R.; Ruiz-Taylor, L.; Textor, M.; Hubbell, J. A.; Spencer, N. D. Poly(L-Lysine)-*g*-Poly(Ethylene Glycol) Layers on Metal Oxide Surfaces: Attachment Mechanism and Effects of Polymer Architecture on Resistance to Protein Adsorption. *J. Phys. Chem. B* **2000**, *104*, 3298−3309.

DOI: 10.1021/acsami.5b01423
ACS Appl. Mater. Interfaces 2015, 7, 10374−10385